Structure and properties of gallate and germanate langasite infrared optical glass materials

Florian Calzavara, Pierre Florian, Franck Fayon, Sonia Buffiere, Marc Dussauze, Veronique Jubera, Thierry Cardinal, Evelyne Fargin

Journal of Non-Crystalline Solids 646 (2024) 123204

Contents lists available at ScienceDirect

Journal of Non-Crystalline Solids

journal homepage: www.elsevier.com/locate/jnoncrysol

Structure and properties of gallate and germanate langasite infrared optical glass materials

Florian Calzavara [a], Pierre Florian [b], Franck Fayon [b], Sonia Buffière [a], Marc Dussauze [c], Véronique Jubera [a], Thierry Cardinal [a], Evelyne Fargin [a,*]

[a] Institut de Chimie de la Matière Condensée de Bordeaux, UMR 5026, 87 Avenue du Dr Schweitzer, Pessac F-33608, France
[b] Conditions Extrêmes et Matériaux: Haute Température et Irradiation, UPR 3079, Université d'Orléans, 1 Avenue de la Recherche Scientifique, 45100 Orléans, France
[c] Institut des Sciences Moléculaires, UMR 5255, Université de Bordeaux, 351 cours de la Libération, Talence Cedex 33405, France

ARTICLE INFO

Keywords:
Oxide glasses
Glass structure
Gallate
Germanate

ABSTRACT

Glasses in the system BaO – La_2O_3 – Ga_2O_3 – GeO_2 and Langasite crystalline phases with the same stoichiometry have been studied considering the possible use of these glasses for laser-induced space-selective growth of crystalline architectures in the glass compositions. For better understanding of mechanisms involved in such controlled crystallization process, crystalline and glass compounds with same stoichiometry and different La/Ba ratios have been synthesized to compare their local structure. Solid-state Nuclear Magnetic Resonance evidence 4- and 5-coordinated gallium units in the glass matrix, denying unambiguously the formation of 6-coordinated gallium sites observed in crystalline phases. Moreover vibrational spectroscopies suggest a link between a 3D network formed by 4- and 5-coordinated gallium, connected to each other and to 4- coordinated Q4 and Q3 germanium units in the glass and their congruent crystallization. The transition from 4- and 5-coordinated gallium to 6-coordinated gallium sites observed in Langasite crystalline phases remains not still elucidated.

1. Introduction

Materials covering a transparency window from the ultra – violet (UV) up to the mid – infrared (MIR) domain are of interest. Gallate-(Ga_2O_3-) and germanate (GeO_2-) based optical glasses are suitable candidates since they exhibit a transparency domain from the UV (~ 280 nm) up to the MIR (~ 5–6 μm) with mechanical assets comparable to silica glasses [1] while being capable to be shaped as sub-millimetric-size as optical glass fibers [2]. In addition, several compositions have demonstrated a promising potential for hosting a relatively large amount of rare-earth emitting centers (*i.e.* ~ 25 Er_2O_3 – 25 La_2O_3 – 50 Ga_2O_3 mol% glass for example [3]) enabling key luminescence properties ranging from the visible up to the MIR [3,4]. Nonetheless, the random atomic arrangement of glasses with an inversion symmetry prevents the generation of active functional properties such as second – order optical nonlinearity or piezoelectricity for example. The crystallization control providing surface or bulk precipitation of crystalline phases in glasses is a well-known method for the development of novel functional materials [5]. In the two recent decades, numerous studies of laser-induced space-selective crystallization of glass and growth of crystalline architectures in glass by direct laser writing have been efficiently realized as reviewed by Komatsu and Honma [6]. These methods open the way to the fabrication of 2D and 3D components of integrated optical circuits in glass matrix which obtain functional properties of crystals such as high second-order susceptibility, linear electrooptic effect, ferroelectricity, etc. For this purpose, the study of controlled crystallization of langasite-type (LGS) crystalline phases has been promoted in this study since their local structure provide a high temperature use while combining optical, electro – optical and multiferroic properties [7–11]. Previously, the langasite-type phases were singly crystallized in the corresponding stoichiometric multicomponent glass systems (BaO – La_2O_3 – Ga_2O_3 – GeO_2) after thermal treatment [12], opening the way for future laser-induced controlled space-selective crystallization [13]. Furthermore, we selected this langasite – type solid solution since the main constituent from those crystal compositions can emerge from germanate to gallate glass network formers. In this glass system the precipitation of single LGS crystalline phase in the glass of composition 16.43 BaO-17.14 $LaO_{3/2}$–40.00 $GaO_{3/2}$–26.43 GeO_2 (at.%) was recently demonstrated [14] and the local structure of the glass matrix was studied by combined high – field solid –

* Corresponding author.
E-mail address: evelyne.fargin@u-bordeaux.fr (E. Fargin).

https://doi.org/10.1016/j.jnoncrysol.2024.123204
Received 29 May 2024; Received in revised form 26 July 2024; Accepted 24 August 2024
Available online 4 September 2024

Table 1
Nominal theoretical and experimental compositions of the corresponding LGS – type $Ba_xGa_{5-x}Ge_{1+x}La_{3-x}O_{14}$ - glass and – crystal materials with $x = 0, 1, 2, 3$. Glass compositions have been measured using induced coupled plasma optical emission spectroscopy (ICP – OES) with a standard deviation of ± 2 at.%. Crystal compositions have been verified by Energy Dispersive X – Ray spectroscopy (EDX) mapping with a standard deviation of ± 2 at.%. "Th" and "Exp" correspond to the abbreviation of "Theoretical" and "Experimental" respectively.

		Nominal cationic molar composition (cat mol %)			
Glass compositions		$GaO_{3/2}$ ± 2%	GeO_2 ± 2%	BaO ± 2%	$LaO_{3/2}$ ± 2%
$La_2BaGa_4Ge_2O_{14}$ – glass	Th	44.44	22.22	11.11	22.22
	Exp	45.(5)	19.(4)	11.(6)	23.(6)
$LaBa_2Ga_3Ge_3O_{14}$ – glass	Th	33.33	33.33	22.22	11.11
	Exp	33.(3)	31.(9)	23.(4)	11.(4)
$Ba_3Ga_2Ge_4O_{14}$ – glass	Th	22.22	44.44	33.33	0
	Exp	22.(4)	43.(7)	34.(0)	–
Crystal compositions	$GaO_{3/2}$ ± 2%	GeO_2 ± 2%	BaO ± 2%	$LaO_{3/2}$ ± 2%	
$La_3Ga_5GeO_{14}$ – crystal	Th	55.56	11.11	0	33.33
	Exp	57.(9)	9.(6)	0	32.(5)
$La_2BaGa_4Ge_2O_{14}$ – crystal	Th	44.44	22.22	11.11	22.22
	Exp	46.(8)	22.(2)	10.(4)	20.(6)
$LaBa_2Ga_3Ge_3O_{14}$ – crystal	Th	33.33	33.33	22.22	11.11
	Exp	37.(9)	28.(8)	19.(6)	13.(8)
$Ba_3Ga_2Ge_4O_{14}$ – crystal	Th	22.22	44.44	33.33	0
	Exp	25.(9)	41.(9)	32.(1)	–

state ^{71}Ga NMR and vibrational spectroscopies. In this paper, the main spectral features in the glasses and the crystalline LGS compounds are investigated.

2. Experimental parts

2.1. Glass synthesis

Glasses were elaborated using high purity powders Ga_2O_3 (Fox Chemicals, ≤ 99.999%), GeO_2 (Fox Chemicals, ≤ 99.999%), La_2O_3 (Stream Chemicals, ≤ 99.99%) and $BaCO_3$ (Fox Chemicals, ≤ 99.99%). Before being weighed out in stoichiometric proportions corresponding to the glass compositions $Ba_xGa_{5-x}Ge_{1+x}La_{3-x}O_{14}$ with $x = 0, 1, 2, 3$. Lanthanum oxide has been pre – heated at a temperature equal to 900 °C for a duration of about 2 h. One notes that the heat treatment of lanthanum oxide have been made since La_2O_3 is very hygroscopic and may also absorb carbonates to form $La_2O_2CO_3$. Thus La_2O_3 suffers significantly from weight changes when used in manufacturing processes as compared to other reagents. The mixtures were then grinded in an agate mortar. Then the powders were placed in the same platinum crucible before being heated up to the melting temperature for a duration of ~ 1–2 h in an electrical furnace with a heating rate of ~ 10 °C.min^{-1}. Melting temperatures were increased from ~ 1450 °C to ~ 1600 °C according to the decrease in the x fraction in order to homogenize the liquid melt. The use of a lot of thermal energy may be justified since gallium-rich germanate glasses possess a combination of unique superior properties which are the mid-infrared transparency up to 5.5 μm, relatively high nonlinear third order optical properties, a glass ability to be shaped as optical fibres and superior mechanical properties and a high rare – earth solubility up to 20–25 mol%. The platinum crucible has been further quenched in water at room temperature. The glasses were taken out of the Pt container by slightly moving the walls of the Pt crucible. Using this method, the glasses gently detached from the crucible walls. Transparent glasses exhibiting a yellowish tint were obtained for LGS – type glasses with $x = 1, 2, 3$. We propose that some platinum from the crucible may be dissolved in the glass as Pt^{4+} during the manufacturing process at high temperatures. This may explain the yellowish tint since platinum as Pt^{4+} presents absorption bands in the visible range at 357 nm and 425 nm [15]. The glass corresponding to the $Ga_5GeLa_3O_{14}$ (at.%) composition could not be obtained even with a melting temperature increased up to ~ 1600 °C. The low amount of glass former GeO_2 can prevent the glass formation of composition $Ga_5GeLa_3O_{14}$ (at.%). The optical glasses were subsequently cut and polished on both parallel faces for further characterizations. Glass compositions have been verified using induced coupled plasma optical emission spectroscopy (ICP – OES) measurement with a standard deviation of ± 2 atomic percent as shown in Table 1. Glass Samples for ICP – OES measurements were prepared by microwave mineralization.

2.2. Crystal synthesis

The $La_3Ga_5GeO_{14}$ LGS phase ($x = 0$) was prepared through classic solid state route. Powder precursors were weighed out in stoichiometric proportions before being carefully grinded in an agate mortar. The powder was subsequently shaped as a pellet before being sintered at 1350 °C during 12 h. The remaining LGS crystals with $x = 1, 2, 3$ belonging to the solid solution $Ba_xGa_{5-x}Ge_{1+x}La_{3-x}O_{14}$ were obtained by congruent crystallization of the previous obtained glasses previously crushed in powder. $BaGa_4Ge_2La_2O_{14}$, $Ba_2Ga_3Ge_3LaO_{14}$, $Ba_3Ga_2Ge_4O_{14}$ were obtained after a heat treatment of 14, 8 and 10 h respectively at a temperature of 1000 °C since it ensures the full glass crystallization. No additional longer thermal treatment has been done in order to verify the full crystallization of the glasses. Crystal compositions have been verified by Energy Dispersive X-Ray spectroscopy (EDX) mapping using a MET JEOL 2200FS with a standard deviation of ± 2 atomic percent.

2.3. Thermal and physical characterizations

Thermal properties including the onset of the glass transition temperature (T_g) and the onset of the crystallization temperature (T_x) were measured on a Netzsch DSC Pegasus 404 F3 apparatus in a platinum pan using glass powder. A heating rate of 10 °C.min^{-1} has been used. The onset of the T_g and T_x were determined from the DSC trace from the tangents crossing. The error has be estimated to be equal to ± 2 °C. The density ρ was obtained from the average of five measurements per sample using Archimedes method by immerging a glass chunk in diethyl phthalate at room temperature on a Precisa XT 220A weighing scale. The estimated errors were estimated around ± 0.01 g.cm^{-3}. Optical properties have been investigated by transmission measurements. The infrared transmission spectra were recorded on a spectrometer Brüker Equinox 55 from 4000 cm^{-1} to 900 cm^{-1} with a spectral resolution of 4 cm^{-1}. The spectra have been recorded from an average of 32 scans. The linear absorption coefficient α has been obtained from the transmission spectra according to the relation $\alpha = -\frac{\ln(I/I_0)}{x}$, where x is the sample's thickness and I/I_0 the transmission percentage. Fresnel reflections have been subtracted. The IR absorption edges were determined for an absorption coefficient equal to $\alpha = 10$ cm^{-1}. The ultraviolet – visible transmission spectra were recorded on a Cary5000 (Varian)

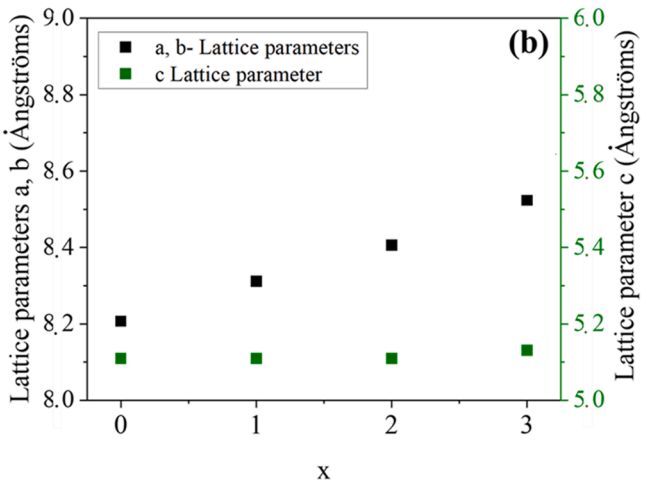

Fig. 1. Evolution of the a –, b – and c – lattice parameters in the solid solution $Ba_xGa_{5-x}Ge_{1+x}La_{3-x}O_{14}$.

from 200 nm to 2500 nm with a spectral resolution of 1 nm. The sample thickness of $Ba_3Ga_2Ge_4O_{14}$ (at.%), $Ba_2Ga_3Ge_3LaO_{14}$ (at.%) and $BaGa_2Ge_4La_2O_{14}$ (at.%) glasses were respectively 0.050 cm, 0.234 cm and 0.047 cm.

2.4. Structural characterizations

The amorphous state of the glass samples was verified by powder X –Ray Diffraction (XRD) which were collected on a PANalitycal X'pert PRO MPD diffractometer used in a Bragg-Brentano θ – θ geometry and equipped with a secondary monochromator and X'Celerator multi –strip detector. Measurements were performed within an angular range of 2θ= 8°–80°. Lebail refinements were performed on crystalline phases. The powders have been sieved to a size of 40 μm. Measurements were performed within an angular range of 2θ= 10.0042° –129.9995° with a step interval equals to 0.008356°. ^{71}Ga solid-state NMR spectra were obtained on a wide bore 20.0 T Bruker Neo spectrometer using a rotor-synchronized solid echo excitation with a full echo acquisition (*i.e.* T_{90} – τ – T_{90} – acq.) to avoid any ambiguity related to phasing and baseline correction. All powdered samples have been packed in 1.3 mm zirconia rotors, spun at 64.0 kHz and the delay set to 12 rotor periods (*i.e.* 187 μs). A short, selective, pulse T_{90} of 0.9 μs has been used at a radio-frequency field of 100 kHz ensuring a full excitation of the spectra. A recycle delays were 0.5 s (spin-lattice relaxation times estimated ≤ 100 ms) and between 8192 and 16,384 transients were accumulated for all compositions. ^{71}Ga chemical shift is referenced to a 1 M solution of $Ga(NO_3)$. All spectra were simulated using DMFit based on either the so-called "Czjzek" (or Gaussian Isotropic) model for glassy compounds or the "Czjzek extended" model for the crystalline one, both models rendering the quadrupolar-broadened central ⟨1/2,−1/2⟩ transition in the finite spinning-speed regime (*i.e.* taking into account its spinning sidebands [16]. Unpolarized Raman spectra were recorded with a confocal micro – Raman spectrometer LabRAM HR Evolution (Horiba Jobin Yvon) equipped with a Synapse CCD detector cooled down to −70 °C using a 532 nm radiation from a diode pumped solid state laser (output power = 20 mW). The incident laser beam was focused onto the sample through a microscope with a 50x objective (NA = 0.50, Olympus). Scattered light was dispersed by 1200 grooves. mm^{-1} grating system. Raman spectra have been corrected by the Bose – Einstein factor. The reflectance infrared spectra of the glasses were recorded with an incident angle of 11° from 200 to 1000 cm^{-1} with a spectral resolution of 4 cm^{-1} using a Fourier Transform Spectrometer Vertex 70 V. A MIR source has been used (globar type). All measurements were performed in vacuum. The spectra have been averaged from 200 measurements. Kramers – Kronig transforms have been performed in order to extract the optical constant k from the imaginary part of the refractive index $\underline{n}$ according to the relation $\underline{n} = n_0 + i\,k$ with n_0 the linear refractive index.

3. Results

3.1. Synthesis

Glass and crystal synthesis are reported in **Section 2**. Nominal theoretical and experimental compositions are presented in Table 1. One observes a relatively good agreement between the targeted and the experimental glass and crystal compositions.

X – Ray diffraction patterns of the langasite crystals obtained either via glass crystallization or classic solid state route in the solid solution $Ba_xGa_{5-x}Ge_{1+x}La_{3-x}O_{14}$ with x = 0, 1, 2, 3 are shown in ref [14] and Supplementary Data. The LGS crystal structure belongs to the structure type of calcium germanate $Ca_3Ga_2Ge_4O_{14}$ consistent with the space group P321. The evolution of the a –, b – and c – lattice parameters reported in Fig. 1. Those parameters have been obtained using the Lebail least square refinements.

In accordance with ref [12], we obtain a linear increase of the lattice parameters while displacing the solid solution from $La_3Ga_5GeO_{14}$ towards $Ba_3Ga_2Ge_4O_{14}$ phases in accordance with the common Vegard's rule. The similar measured composition (Table 1) between the glass and the crystal and the linear evolution of the lattice parameters suggests a congruent crystallization. The increase in the a-, b-, c- lattice parameters with x can be mostly ascribed to the larger ionic radius of Ba^{2+} (r^{2+}_{Ba}= 1.38 Å [17]) than La^{3+} (r^{3+}_{La}= 1.05 Å [17]) involving more drastic evolution on a-, b- lattice parameters. However a contradiction appears considering the larger ionic radius of gallium in tetrahedral or octahedral environment compared to germanium ionic radius in the same site. Indeed LGS phases are reported in the chemical formula $A_3BC_3D_2O_{14}$ where A and B cations are respectively located on decahedral site (3e) and octahedral site (1a) while C and D are located in tetrahedral site respectively 3f and 2d Wyckoff's positions [18]. In $La_3Ga_5GeO_{14}$, Ge is mostly located in 2d smaller tetrahedral site whereas in compositions with larger ratio Ge/Ga like $Ca_3Ga_2Ge_4O_{14}$ or $Sr_3Ga_2Ge_4O_{14}$, Ge is also

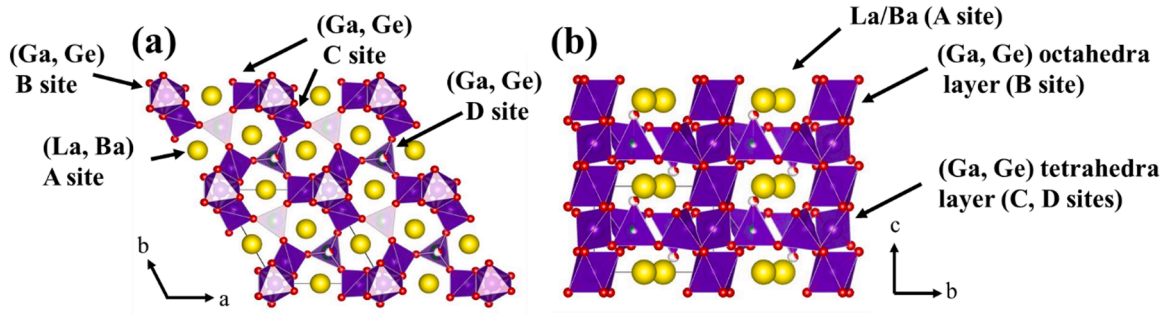

Fig. 2. $La_3Ga_5GeO_{14}$ crystalline phases obtained from the refined XRD pattern according to the (a) a – b and (b) b – c planes.

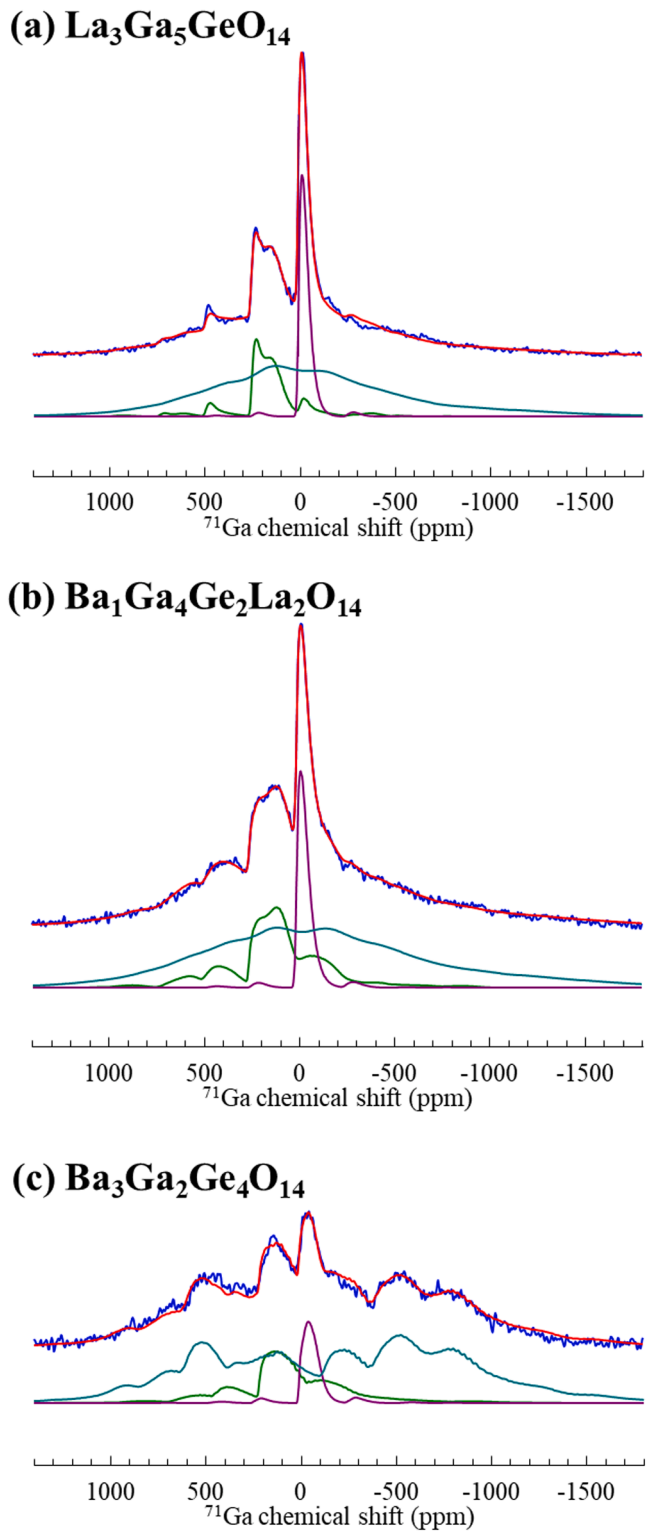

Fig. 3. ^{71}Ga Solid – State Nuclear Magnetic Resonance (SSNMR) spectra of the crystalline compositions (a) $La_3Ga_5GeO_{14}$ (b) $Ba_1Ga_4Ge_2La_2O_{14}$ (c) $Ba_3Ga_2Ge_4O_{14}$. The $La_3Ga_5GeO_{14}$ crystalline phase spectra is identical to the one already published under similar experimental conditions assigned to only GaO_4 and GaO_6 coordinated gallium units [22].

expected in larger site [19]. LGS crystal structure can then be described by layers formed with six membered rings made of three CO_4 and two DO_4 tetrahedrons, bonded to each other by the edges to one BO_6 octahedron. The CO_4 tetrahedrons have only bridging oxygen anions while DO_4 tetrahedrons have one nonbridging oxygen anion. Eight coordinated La^{3+} or Ba^{2+} cations occupy AO_8 sites in between the tetrahedral layers. As an illustration, the $La_3Ga_5GeO_{14}$ LGS structure is presented in Fig. 2a–b. The nature of the atoms (Ga, Ge) position in their sites evolves according to the increasing Ge/Ga ratio with x in the solid solution $Ba_xGa_{5-x}Ge_{1+x}La_{3-x}O_{14}$. According to ref [19], we suggest that the decrease of AO_8vol with x decrease could be ensured thanks to exchanges of Ge between 2d and 1a sites and a great volume flexibility of 3f sites when occupied by Ga, with different result on (a-, b-) and c- cell parameters.

The ^{71}Ga NMR spectrum of $La_3Ga_5GeO_{14}$ shows a very complex line shape pattern (Fig. 3a) arising from strong electric field gradients felt by this nuclei. A very reasonable decomposition can nevertheless be obtained, using the so-called "extended-Czjzek" model, *i.e.* taking into account a random distribution of quadrupolar interaction around a well-defined set of (C_Q, η_Q) values. In other words this an attempt to simulate small local structural variations at well-defined crystallographic sites, a procedure which has been successfully applied in the case of ^{139}La NMR in $La_2Si_2O_7$-$Y_2Si_2O_7$ solid solution [20]. Under this assumption, the simulation reveals three components with respective isotropic chemical shifts of 10 ppm, 279 ppm and 233 ppm and based on those numbers the first component is assigned to the GaO_6 site in 1a (site B). The two other components are then expected to be GaO_4 units, and this is confirmed by their high isotropic chemical shift values. They are markedly different not only in their C_Q values (resp. 17.2 Mhz and 25.5 MHz), but also in their integrated intensity (resp. 18 % and 64 %) leading to an overall population very close to 20 %:20 %:60 % ratios for the three sites, in excellent agreement with the 1:1:3 expected ratio for the 1a:2d:3f sites when taking into account the partial occupancy of the 2d one. We therefore assign the (233 ppm, 25.5 MHz) site to GaO_4 in 3f position (site C) and the (279 ppm, 17.2 MHz) one to GaO_4 in 2d position (site D). It is striking to observe a C_Q value as high as 25.5 MHz and it suggests a highly distorted GaO_4 tetrahedra [21], again in agreement with the crystallographic data and the distribution of O–Ga–O bond angle found for this 3f site (site C) as opposed to the more symmetric 2d site (site D). It is worth noting that only the 3f (site C) site sees the $(Ga,Ge)O_4$ partial occupancy of the 2d site (site D) as a second neighbor and is connected to GaO_6 units, which leads to even more structural distortion than the average picture given by the XRD analysis. On the other hand, the presence of one non-bridging oxygen on the 2d (site D) site does not lead to a significant increase in the distortion of this GaO_4 tetrahedra.

The ^{71}Ga NMR spectra of $BaLa_2Ga_4Ge_2O_{14}$ (Fig. 3b) bears strong resemblance with that of $La_3Ga_5GeO_{14}$ with an increased importance of the disordered contribution to the electric field gradient (as measured with the ε parameter), in agreement with the increased configurational degree of freedom induced by the presence of Ba atoms in the structure. While the relative intensities are staying the same suggesting a similar structure, one observes a significant increased shielding (downward shift of –30 ppm) of the isotropic chemical shift for the 3f sites (site C). This is also the case for the $Ba_3Ga_2Ge_4O_{14}$ (Fig. 3c) compound, with an additional deviation from the 1:1:3 initial ratio between the crystallographic sites. Fitting parameters are given in Table 2.

3.2. *Glass physico – chemical properties*

Glass thermal properties and their density are presented in Table 3. The glass transition temperatures T_g increase from 665 °C to 738 °C upon the x decrease in the glass system $Ba_xGa_{5-x}Ge_{1+x}La_{3-x}O_{14}$.The density increases as well from 4.87 g.cm^{-3} up to 5.34 g.cm^{-3}. Such variations could be characteristic of important changes in the network glass structure.

A transparent region from the UV (~ 280 nm) up to the mid infrared (MIR) domain is observed for the glass $Ba_3Ga_2Ge_4O_{14}$ in Fig. 4. The linear absorption coefficient α in the MIR window is reported in inset. All glass present an IR transparency up to 5.5–6 μm due to the low phonon energy compounds Ga_2O_3 (~ 650 cm^{-1}) and GeO_2 (~

Table 2
SSNMR parameters from line shape fitting of the investigated langasite – type glasses.

Crystalline sample	Wyckoff position (Site)	Proportion (%)	δ_{iso} (ppm)	$\Delta\delta_{iso}$ (ppm)	C_Q (MHz)	ΔC_Q (MHz)	η_Q	ε
$La_3Ga_5GeO_{14}$	2d	18	279.0	5.8	17.18	4.66	0.15	0.15
	1a	18	10.3	17.3	9.44	6.20	0.65	0.15
	3f	64	232.7	173.5	25.48	10.96	0.0	0.90
$BaGa_4Ge_2La_2O_{14}$	2d	24	268.8	12.1	19.08	4.69	0.15	0.90
	1a	14	15.7	19.3	10.54	6.99	0.65	0.15
	3f	62	203.6	173.5	27.78	11.93	0.2	0.90
$Ba_3Ga_2Ge_4O_{14}$	2d	18	221.4	11.6	19.89	8.05	0.20	0.90
	1a	7	14.2	11.6	13.32	4.17	0.50	0.20
	3f	75	164.2	11.6	30.67	5.74	0.30	0.20

Table 3
Thermal properties and density of the corresponding langasite – type $Ba_xGa_{5-x}Ge_{1+x}La_{3-x}O_{14}$ glasses.

	T_g (± 2 °C)	T_x (± 2 °C)	$\Delta T = T_x - T_g$ (± 4 °C)	P (± 0.01 g. cm^{-3})
$Ba_1Ga_4Ge_2La_2O_{14}$	738	834	96	5.34
$Ba_2Ga_3Ge_3La_1O_{14}$	718	840	122	4.98
$Ba_3Ga_2Ge_4O_{14}$	665	777	112	4.87

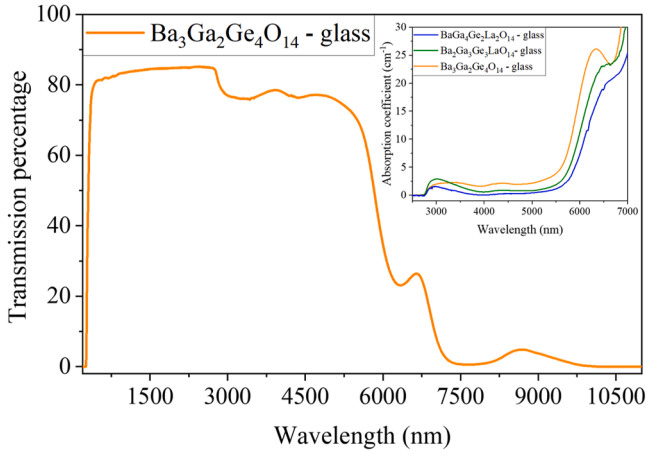

Fig. 4. Transmission spectrum of the germanate stoichiometric $Ba_3Ga_2Ge_4O_{14}$ glass. The linear absorption coefficient α in the mid – infrared range from 2500 nm up to 7000 nm of the langasite – type glass samples are shown in the inset.

900 cm^{-1}). Several absorption bands located around ~ 3300 nm, ~ 4400 nm, ~ 6400 nm and ~ 7600 nm can be noticed. The absorption band located around ~ 3300 nm and the absorption band located at ~ 4400 nm could be characteristic of Ge–OH or Ga–OH combined stretching and bending vibration modes with the hydrogen being either strong or very strong bonded [23]. The assignation of the absorption bands located at higher wavelengths (~ 6400 nm and ~7600 nm) could be characteristic of overtones corresponding to fundamental IR vibrational modes [24].

One observes two main effects upon the x decrease in the $Ba_xGa_{5-x}Ge_{1+x}La_{3-x}O_{14}$ solid – solution: *(i)* a change in the line shape of the absorption band located at ~ 3300 nm combined with a decrease of the absorption band located around ~ 4400 nm and *(ii)* a red-shift of the IR absorption edge from ~ 5800 nm up to ~ 6100 nm for a linear absorption coefficient α equals to 10 cm^{-1} upon the compositional change from langasite barium germanate ($x = 3$) to the lanthanum gallate ($x = 1$). Spectral differences can be mostly assigned to an important modification in the glass structure from the germanate – rich to the gallate – rich glass skeleton.

3.3. Glass structural properties

3.3.1. Solid – state nuclear magnetic resonance spectroscopy

^{71}Ga solid-state Nuclear Magnetic Resonance (SSNMR) spectra collected at high magnetic field (20.0 T) and very fast spinning (64 kHz) are presented in Fig. 5a–c, along with some of their crystalline counterpart when available. The differences in the spectra obtained for the glasses and the crystals are striking: GaO_6 environments are clearly absent from the $BaLa_2Ga_4Ge_2O_{14}$ glass, and the GaO_4 site with large C_Q is, within a few percent, not seen in $Ba_3Ga_2Ge_4O_{14}$. In order to better understand those spectral variations, deconvolution of the characteristic line shapes are made using the so-called "Czjzek" model applicable to half-integer nuclei in fully randomly disordered environments. As can be seen in the Fig. 5a–c, those latter ones are dominated one main peak with a maximum around 180 ppm and a discontinuity around 70 ppm [25–28]. Assuming the presence of only two sites leads to an excellent simulation of the experimental spectrum, including the spinning sidebands, which points to GaO_4 (δ_{iso}~ 210 ppm) and GaO_5 (δ_{iso}~ 110 ppm) types of environments and the absence of GaO_6 units (which isotropic chemical shifts are around 50–60 ppm) [25–28]. The absence of the later can be related to the absence of GaO_6 units in the glass and to which this site was connected in the crystalline compounds. As seen in Table 4, those simulations show that upon increasing the La/Ba ratio the GaO_4 site is decreasing with respect to GaO_5, and both sites average (most probable) isotropic chemical shifts move to higher values (decreasing shielding). This chemical shift change can be assigned to a change in the nature of the second coordination sphere neighbor of Ga, and hence to the changes in the nature of the cation performing the charge compensation of the (Ga,Ge)–O–(Ga,Ge) glass skeleton. The obtained fitting parameters indicate that the x decrease from 3 to 1 in the glass compositions $Ba_xGa_{5-x}Ge_{1+x}La_{3-x}O_{14}$ leads to increase significantly the fraction of GaO_5 units of about ~ 5% up to ~ 24%. This important increase in the GaO_5 fraction can be partly explained due to the higher cationic field strength Z defined as the ratio of the cationic charge out of the ionic radius of Lanthanum ($Z = 2.72$ Å^{-2} [17]) as compared to Barium cations ($Z = 1.05$ Å^{-2} [17]). This increased the structural disorder with higher field strength cation is confirmed with the increase of σ_c with increasing La content since σ_c^2 is the variance of the distribution of the quadrupolar interaction and hence measures the extent of the atomic-level disorder present in the sample.

3.3.2. Vibrational spectroscopy

Unpolarized Raman and Fourier Transformed InfraRed (FTIR) spectra of the investigated langasite – type glasses are presented in Fig. 6a–b. Those spectra were respectively normalized with respect to their total area between 200 cm^{-1} and 1000 cm^{-1}. A perfect agreement on Fig. 6a- is observed with Raman spectra obtained by [12] for $x = 1$ and $x = 3$ while the spectrum for $x = 2$ is of better quality unlike it was polluted by a weak Eu^{3+} photoluminescence. Then a continuous evolution of FTIR and Raman spectra can be insured for x increasing from 1 to 3. These spectra can be usually decomposed in three main regions which correspond respectively to the frequency domains between 200–430 cm^{-1}, 430–600 cm^{-1} and 600–1000 cm^{-1}. The lowermost

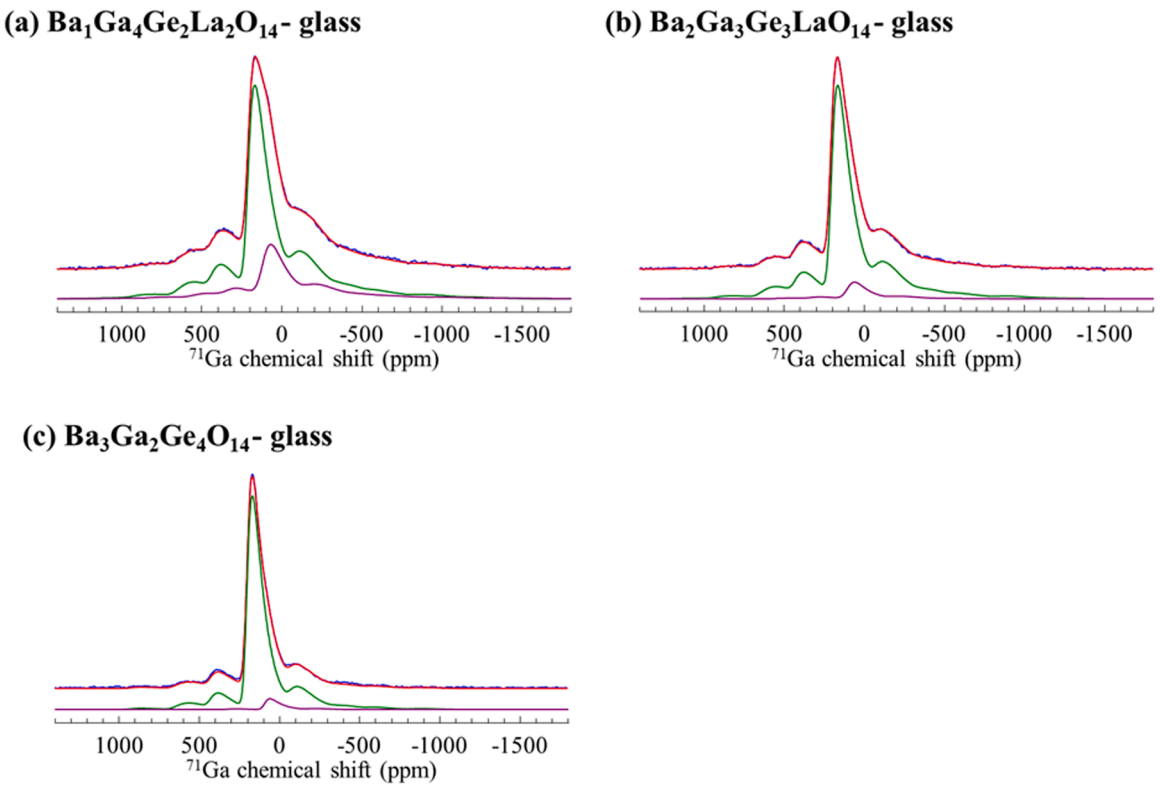

Fig. 5. ^{71}Ga Solid – State Nuclear Magnetic Resonance (SSNMR) spectra of the glass compositions (a) $BaGa_4Ge_2La_2O_{14}$ (b) $Ba_2Ga_3Ge_3LaO_{14}$ (c) $Ba_3Ga_2Ge_4O_{14}$.

Table 4
SSNMR parameters from line shape fitting of the investigated langasite – type glasses.

Glass sample	Coordination number	Proportion (%)	δ_{iso} (ppm)	$\Delta\ \delta_{iso}$ (ppm)	σ_C (MHz)
$Ba_3Ga_2Ge_4O_{14}$ - glass	4	95	207.2	42.9	7.58
	5	5	97.2	42.4	7.50
$Ba_2Ga_3Ge_3LaO_{14}$ - glass	4	93	213.4	49.0	8.75
	5	7	113.9	68.4	8.24
$BaGa_4Ge_2La_2O_{14}$ - glass	4	76	217.0	52.8	9.52
	5	24	126.9	77.8	10.0

200–430 cm^{-1} region is often assigned to vibrational signature of heavy cations such as barium and lanthanum oxide in an oxygenated site [29–31]. The intermediate frequency window between 400–600 cm^{-1} is mainly characteristic to a combination of stretching ν (T–O–T) and bending δ (T–O–T) modes of an oxygen surrounded by two units being either gallate or germanate ones. The highest frequency region between 600–1000 cm^{-1} contains mainly localized stretching features of germanium sites involved respectively in $Q_{n=1,2,3,4}$ germanate units [32] and gallate –based polyhedra units [14,29,33]. This regions contains also stretching frequencies of an oxygen surrounded by gallate and/or germanate units ν ($T^{[4]}$ –O–$T^{[4]}$) bridges [34,35] and Ga–O vibrations in $GaO_{4,5}$ polyhedra including probably a non – bridging oxygen O_{nb} [14, 29]. According to the spectral variations, one observes that the decrease of x from 3 to 1 in the langasite-type $Ba_xGa_{5-x}Ge_{1+x}La_{3-x}O_{14}$ compositions leads to: *(i)* broaden the vibrational signatures located in the low frequency region, *(ii)* shift the intermediate vibrational band from ~ 512 cm^{-1} to ~ 526 cm^{-1} Raman and from ~ 537 cm^{-1} to ~ 508 cm^{-1} IR signatures in the intermediate frequency region and *(iii)* decrease the intensity and to shift the high frequency peak from ~ 817 cm^{-1} to ~ 793 cm^{-1} and from ~ 769 cm^{-1} to ~ 725 cm^{-1} for Raman and IR signatures respectively. This vibrational changes appears for the benefit of a new signature in the 600 cm^{-1}–700 cm^{-1} range.

3.3.3. Raman comparative analysis with langasite crystal phases

Unpolarized Raman scattering spectra measured on the langasite-type glasses and crystallized phases are shown in Fig. 7. As observed by [12] the vibrational signature of the langasite crystal phases can be superposed with the corresponding glass ones, suggesting similar short range order in the glass structure.

In the low frequency region related to the $Ba_3Ga_2Ge_4O_{14}$ langasite crystal, three main vibrational modes located around ~ 267 cm^{-1}, ~ 300 cm^{-1}, ~ 337 cm^{-1} that could be assigned to Ba–O vibrational modes. Upon the x decrease from 3 to 0 in the glass system $Ba_xGa_{5-x}Ge_{1+x}La_{3-x}O_{14}$, one observes a broadening and a shift of those Raman vibrational modes upon the introduction of lanthanum cations. The appearance of those vibrational modes around ~ 240 cm^{-1} and ~ 324 cm^{-1} can be assigned mostly to stretching La–O vibrational modes [29–31].

Regarding the intermediate frequency region, one observes two main vibrational modes around ~ 487 cm^{-1} and ~ 559 cm^{-1} in the $Ba_3Ga_2Ge_4O_{14}$ Raman spectrum that could be respectively assigned to a combination of stretching and bending vibrational modes of $T^{[4]}$–O–$T^{[4]}$ bridges with T = Ga, Ge corner – shared tetrahedra and $T^{[4]}$–O–$T^{[6]}$ edge – share tetrahedra and octahedra units [36]. Those vibrational peaks shifts from ~ 487 cm^{-1} to ~ 499 cm^{-1} and from ~ 559 cm^{-1} to ~ 590 cm^{-1} upon the x decrease. This may traduce a change in the network connectivity from $Ge^{[4]}$–O–$Ge^{[4]}$ and $Ge^{[4]}$–O–$Ge^{[4,6]}$ in the germanate $Ba_3Ga_2Ge_4O_{14}$ composition to $T^{[4]}$–O–$T^{[4]}$ and $T^{[4]}$–O–$T^{[4,6]}$ bridges in the gallate $La_3Ga_5GeO_{14}$.

Regarding the high frequency region, on the $Ba_3Ga_2Ge_4O_{14}$ Raman spectrum two main strong active intense bands around ~ 813 cm^{-1} and ~ 800 cm^{-1}. According to a previous study [35], one mostly assigns those vibration modes to Q_3 germanate units. Upon the x decrease, several spectral variations which can be described as follows *(i)* a shift from ~ 863 cm^{-1} to ~ 824 cm^{-1} of the most intense vibrational band and *(ii)* an increase of the vibrational modes located in the 600–700 cm^{-1} regions. Based on those spectral variations, both previous items can be mostly ascribed to a change in the crystal skeleton from

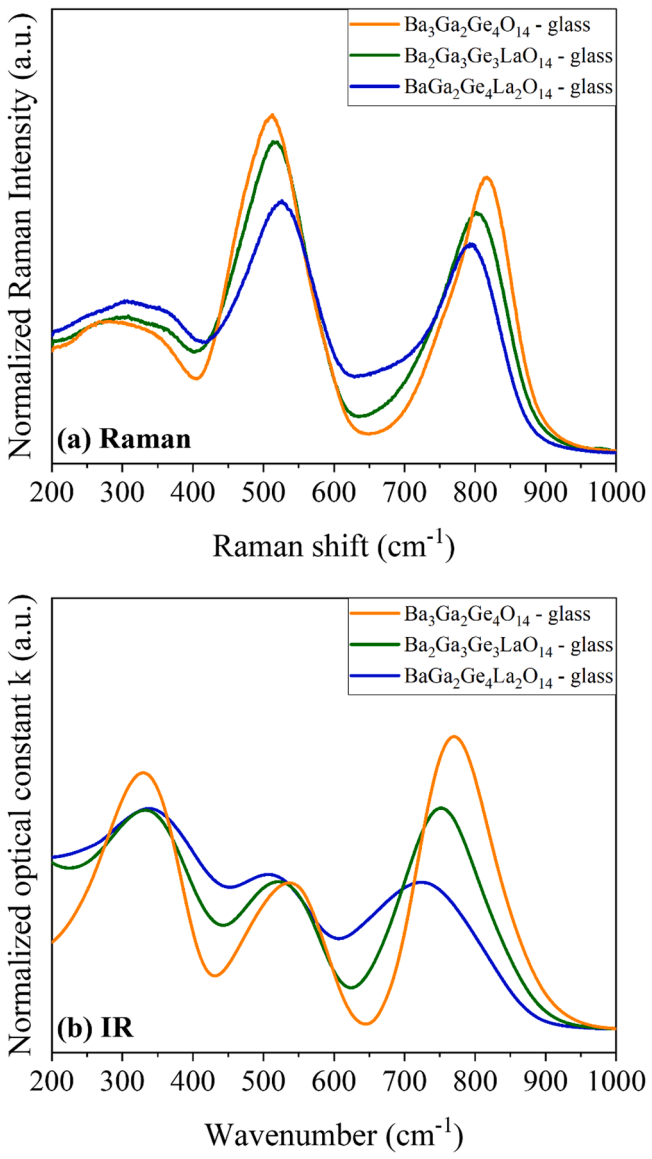

Fig. 6. Vibrational (a) Raman and (b) FTIR spectra of the investigated LGS glass compositions.

germanate (Ge–O–Ge) to gallate –based (Ga–O–Ga) structure with the disappearance of the vibrational modes in the 800–900 cm^{-1} domain. The spectral variations in the 600–700 cm^{-1} region were mostly assigned to the diverse coordination environments of the oxygen atoms in a gallium-rich glass according to Yoshimoto et al. [29,33]. The authors [12] suggested the presence of the octahedral GaO_6 units in the $La_3Ga_5GeO_{14}$ – $Ba_3Ga_2Ge_4O_{14}$ system glass, as would be expected from the crystal structure of the langasite-type phase and concluded to the coexistence of octahedral GaO_6 and GeO_4 units in the gallo-germanate glasses. The present NMR analysis of glass compositions infirm this conclusion since no GaO_6 units have been evidenced in the glasses, thus proving the increase in the pentahedral to tetrahedral units ratio of gallium GaO_5/GaO_4 when Ba is substituted to La. Then the increase of the 600–700 cm^{-1} band intensity can be definitely correlated to the evolution of this ratio.

4. Summary

Heavy Metal Oxide germanate and gallate oxide langasite-type compositions in the system $Ba_xGa_{5-x}Ge_{1+x}La_{3-x}O_{14}$ with $x = 0, 1, 2, 3$ were successfully synthesized either by glass recrystallization or the traditional solid-state route with relatively good agreement factors. In accordance with the refined crystalline structures with $x = 0$ and $x = 1$, those ones can be described as a layered structure including mainly corner-shared GaO_4 tetrahedra perpendicular to the crystallographic c-axis connected through their vertices. These layers are connected by octahedrally coordinated GaO_6 in which eighthly-coordinated Lanthanum or Barium lie, separating then the tetrahedra layers. Similar vibrational signatures can be observed between both crystalline and glass compositions, suggesting the local glass structure contains similar local ordering than the corresponding crystal. In particular, one has observed characteristic vibrational signature of corner-shared oxygenated gallate and/or germanate tetrahedra units. This similar short range order is also consistent with the SSNMR data in which most gallium are found to be four-coordinated. Nonetheless, the large number of GaO_5 around 24 percent units in the glass matrix $Ba_1Ga_4Ge_2La_2O_{14}$ as compared to the $Ba_xGa_{5-x}Ge_{1+x}La_{3-x}O_{14}$ compositions in which with $x = 2$ and 3 can be mostly ascribed to the increase of lanthanum oxide in the glass matrix which presents a higher field strength (~ 2.72 $Å^{-2}$) as compared to barium (~ 1.05 $Å^{-2}$) cations. This increase in highly coordinated gallate GaO_5 units leads to increase significantly the glass transition temperature values as well as a higher glass packing density. Those structural changes from GaO_4 to GaO_5 units when adding La^{3+} ions are thus in good agreement with the increase of the glass transition temperatures and the densities, favoring the glass network polymerization. Furthermore, such increase seems to favor the glass crystallization as can be seen with the reduction of the ΔT values upon the introduction of lanthanum. In opposition to the conclusions of the authors in ref [12], NMR characterization of the glass matrix evidenced 4- and 5-coordinated gallium units and denied unambiguously the formation of 6-coordinated gallium sites [12].

5. Conclusion

Following our previous work [2,14,35], we investigated the properties and the local glass structure of $Ba_xGa_{5-x}Ge_{1+x}La_{3-x}O_{14}$ compositions with $x = 0, 1, 2, 3$ in the glass system $BaO – La_2O_3 – Ga_2O_3 – GeO_2$ considering the optical properties that can be induced by the controlled crystallization of the single Langasite phase having the same stoichiometry. NMR characterization of the glass matrix has evidenced 4- and 5-coordinated gallium units in glasses and denied unambiguously the formation of 6-coordinated gallium sites existing in the crystalline phases. According to vibrational spectroscopies, the glass network can be considered as a 3D network formed by 4- and 5- coordinated gallate units connected to 4- coordinated germanate units. Interconnection between gallate units and the diverse environments of gallium can be at the origin of congruent crystallization towards Langasite phases, though the transition from 4- and 5-coordinated gallium to 6-coordinated gallium sites observed in crystalline phases is not still elucidated.

CRediT authorship contribution statement

Florian Calzavara: Writing – review & editing, Writing – original draft, Visualization, Validation, Methodology, Investigation, Formal analysis, Conceptualization. **Pierre Florian:** Writing – review & editing, Writing – original draft, Visualization, Validation, Supervision, Resources, Methodology, Investigation, Formal analysis. **Franck Fayon:** Writing – review & editing, Visualization, Supervision, Resources, Investigation, Formal analysis. **Sonia Buffière:** Writing – review & editing, Visualization, Validation, Investigation, Formal analysis. **Marc Dussauze:** Writing – review & editing, Visualization, Validation, Resources, Methodology, Funding acquisition, Formal analysis. **Véronique Jubera:** Writing – review & editing, Visualization, Validation, Supervision, Resources, Project administration, Methodology, Funding acquisition, Formal analysis, Conceptualization. **Thierry Cardinal:** Writing – review & editing, Visualization, Validation, Supervision,

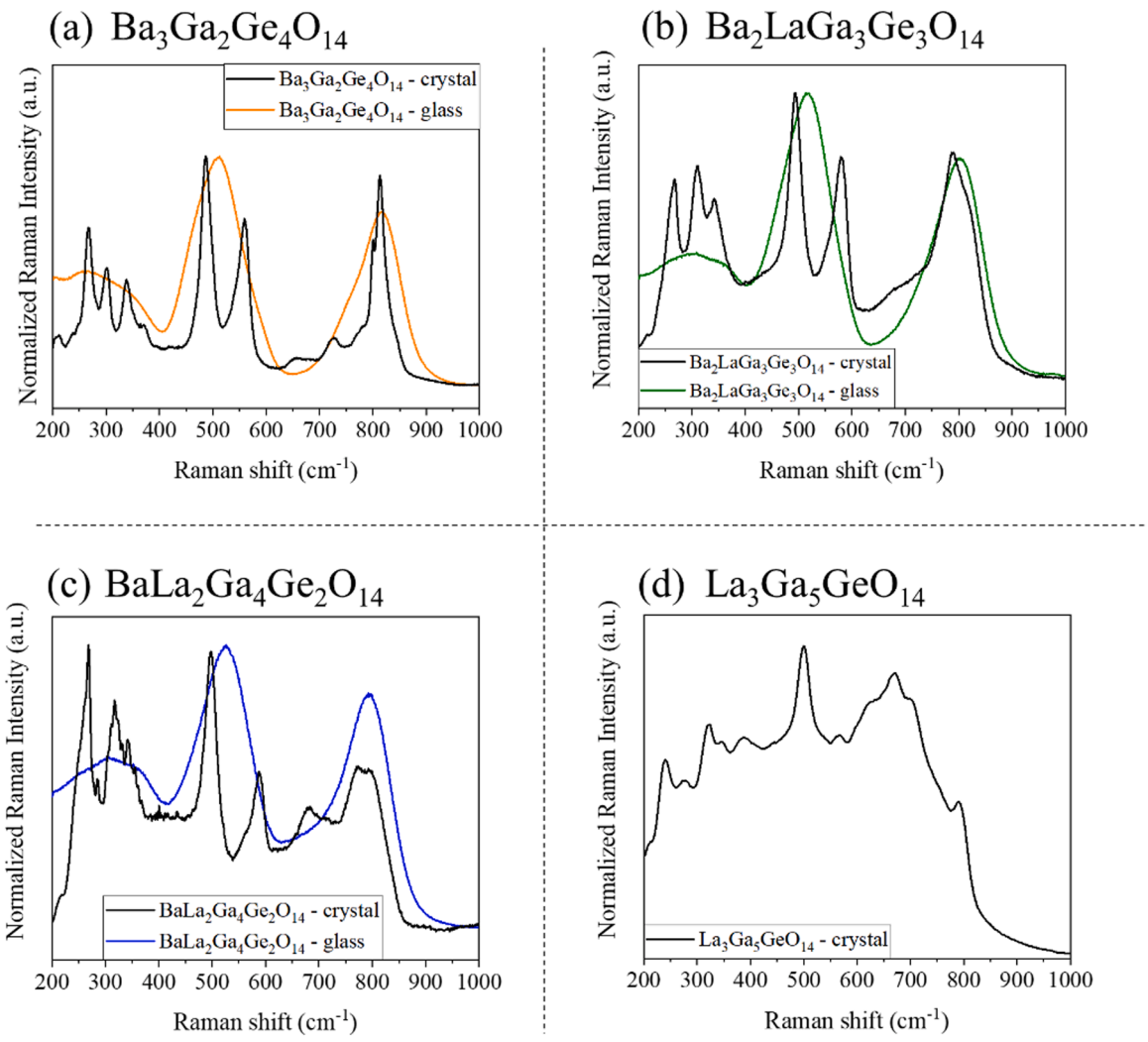

Fig. 7. Raman scattering spectra of the langasite – type crystallized and glass compositions.

Resources, Project administration, Methodology, Investigation, Funding acquisition, Formal analysis, Conceptualization. **Evelyne Fargin:** Writing – review & editing, Visualization, Validation, Supervision, Resources, Project administration, Methodology, Investigation, Funding acquisition, Formal analysis, Conceptualization.

Declaration of competing interest

The authors declare that they have no known competing financial interests or personal relationships that could have appeared to influence the work reported in this paper.

Data availability

No data was used for the research described in the article.

Acknowledgement

Financial support from the IR INFRANALYTICS FR2054 for conducting the research is gratefully acknowledged.

Supplementary materials

Supplementary material associated with this article can be found, in the online version, at doi:10.1016/j.jnoncrysol.2024.123204.

References

[1] C. Strutynski, et al., Heavy-oxide glasses with superior mechanical assets for nonlinear fiber applications in the mid-infrared, Opt. Mater. Express 11 (2021) 1420.
[2] T. Guérineau, et al., Extended germano-gallate fiber drawing domain: from germanates to gallates optical fibers, Opt. Mater. Express 9 (2019) 2437.
[3] K. Yoshimoto, Y. Ezura, M. Ueda, A. Masuno, H. Inoue, 2.7 μm Mid-infrared emission in highly erbium-doped lanthanum gallate glasses prepared via an aerodynamic levitation technique, Adv. Opt. Mater. 6 (2018) 1701283.
[4] K. Yoshimoto, et al., Fluorescence characterization of heavily Eu^{3+} -doped lanthanum gallate glass spheres with high quenching concentration, Opt. Lett. 44 (2019) 875.
[5] T. Komatsu, Design and control of crystallization in oxide glasses, *J. Non-Cryst. Solids* 428 (2015) 156–175.
[6] T. Komatsu, T. Honma, Laser patterning and growth mechanism of orientation designed crystals in oxide glasses: a review, J. Solid State Chem. 275 (2019) 210–222.
[7] H. Kong, et al., Growth, properties and application as an electrooptic Q-switch of langasite crystal, *J. Cryst. Growth* 254 (2003) 360–367.
[8] N. Araki, et al., Origin of piezoelectricity for langasite A3Ga5SiO14 (A=La and Nd) under high pressure, J. Eur. Ceram. Soc. 27 (2007) 4099–4102.
[9] H. Lan, et al., Langasite family midinfrared nonlinear optical oxide materials: structure, property, and applications, Int. J. Opt. 2017 (2017) 1–13.
[10] H. Fritze, H.L. Tuller, H. Seh, G. Borchardt, High temperature nanobalance sensor based on langasite, Sens. Actuators B Chem. 76 (2001) 103–107.
[11] H. Seh, H.L. Tuller, H. Fritze, Langasite for high-temperature acoustic wave gas sensors, Sens. Actuators B Chem. 93 (2003) 169–174.

[12] Y. Takahashi, et al., Crystallization and Raman spectra of langasite-type phases in glasses of $La_3Ga_5GeO_{14}$–$Ba_3Ga_2Ge_4O_{14}$ System, *Jpn. J. Appl. Phys.* 44 (2005) 7177–7181.
[13] S.V. Lotarev, A.S. Lipatiev, T.O. Lipateva, E.V. Lopatina, V.N. Sigaev, Ultrafast laser-induced crystallization of lead germanate glass, Crystals 11 (2021) 193.
[14] F. Calzavara, et al., Resolved-detrimental surface crystallization in yttrium lanthanum gallate glasses for optical fiber applications, *J. Am. Ceram. Soc.* jace (2023) 19184, https://doi.org/10.1111/jace.19184.
[15] C.A. Click, R.K. Brow, P.R. Ehrmann, J.H. Campbell, Characterization of Pt^{4+} in alumino-metaphosphate laser glasses, *J. Non-Cryst. Solids* 319 (2003) 95–108.
[16] D. Massiot, et al., Modelling one- and two-dimensional solid-state NMR spectra, *Magn. Reson. Chem.* 40 (2002) 70–76.
[17] J.M. Jewell, P.L. Higby, I.D Aggarwal, Properties of BaO-R2O3- Ga2O3-GeO2 (R = Y, Al, La, and Gd) Glasses, J. Am. Ceram. Soc. 77 (1994) 697–700.
[18] A.A. Kaminskii, et al., Pure and Nd3+-doped Ca3Ga2Ge4O14 and Sr3Ga2Ge4O14 single crystals, their structure, optical, spectral luminescence, electromechanical properties, and stimulated emission, Phys. Status Solidi A 86 (1984) 345–362.
[19] A.P. Dudka, Multicell model of La3Ga5GeO14 crystal: a new approach to the description of the short-range order of atoms, *Crystallogr. Rep.* 62 (2017) 374–381.
[20] A.J. Fernández-Carrión, M. Allix, P. Florian, M.R. Suchomel, A.I. Becerro, Revealing structural detail in the high temperature $La_2Si_2O_7$–$Y_2Si_2O_7$ phase diagram by synchrotron powder diffraction and nuclear magnetic Resonance Spectroscopy, J. Phys. Chem. C 116 (2012) 21523–21535.
[21] J. Autschbach, S. Zheng, R.W. Schurko, Analysis of electric field gradient tensors at quadrupolar nuclei in common structural motifs, *Concepts Magn. Reson. Part A* 36A (2010) 84–126.
[22] M. Diaz-Lopez, et al., Interstitial oxide ion conductivity in the langasite structure: carrier trapping by formation of $(Ga,Ge)_2O_8$ Units in $La_3Ga_{5-x}Ge_{1+x}O_{14+x/2}$ ($0 < x \leq 1.5$), Chem. Mater. 31 (2019) 5742–5758.
[23] J.M. Jewell, I.D. Aggarwal, Structural influences on the hydroxyl spectra of barium gallogermanate glasses, *J. Non-Cryst. Solids* 181 (1995) 189–199.
[24] G. Guery, et al., Influence of Hydroxyl group on IR transparency of tellurite-based glasses, Int. J. Appl. Glass Sci. 5 (2014) 178–184.
[25] Massiot, D. et al. 71Ga NMR of reference GaIV, GaV, and GaVI compounds by MAS and QPASS, extension of galliumraluminum NMR parameter correlation. 11 (1999).
[26] S.M. Bradley, R.F. Howe, R.A. Kydd, Correlation between27Al and71Ga NMR chemical shifts, *Magn. Reson. Chem.* 31 (1993) 883–886.
[27] C.O. Areán, M.R. Delgado, V. Montouillout, D. Massiot, Synthesis and characterization of spinel-type gallia-alumina solid solutions, *Z. Für Anorg. Allg. Chem.* 631 (2005) 2121–2126.
[28] J.T. Ash, P.J. Grandinetti, Solid-state NMR characterization of ^{69}Ga and ^{71}Ga in crystalline solids, *Magn. Reson. Chem.* 44 (2006) 823–831.
[29] K. Yoshimoto, et al., Principal vibration modes of the La_2O_3–Ga_2O_3 binary glass originated from diverse coordination environments of oxygen atoms, J. Phys. Chem. B 124 (2020) 5056–5066.
[30] T. Skopak, et al., Properties, structure and crystallization study of germano-gallate glasses in the Ga2O3-GeO2-BaO-K2O system, *J. Non-Cryst. Solids* 514 (2019) 98–107.
[31] T. Skopak, et al., Structure-properties relationship study in niobium oxide containing GaO3/2-LaO3/2-KO1/2 gallate glasses, Mater. Res. Bull. 112 (2019) 124–131.
[32] G.S. Henderson, L.G. Soltay, H.M. Wang, Q speciation in alkali germanate glasses, *J. Non-Cryst. Solids* 356 (2010) 2480–2485.
[33] K. Yoshimoto, et al., Low phonon energies and wideband optical windows of La2O3-Ga2O3 glasses prepared using an aerodynamic levitation technique, Sci. Rep. 7 (2017).
[34] T. Skopak, et al., Structure and properties of gallium-rich sodium germano-gallate glasses, J. Phys. Chem. C 123 (2019) 1370–1378.
[35] F. Calzavara, et al., Glass forming regions, structure and properties of lanthanum barium germanate and gallate glasses, *J. Non-Cryst. Solids* 571 (2021) 121064.
[36] E.I. Kamitsos, Y.D. Yiannopoulos, M.A. Karakassides, G.D. Chryssikos, H. Jain, Raman and Infrared Structural Investigation of xRb2O·(1 − x)GeO2 Glasses, J. Phys. Chem. 100 (1996) 11755–11765.